Article

Localized Surface Plasmon Resonance Sensing of Lipid-Membrane-Mediated Biorecognition Events

Andreas Dahlin, Michael Zch, Tomas Rindzevicius, Mikael Kll, Duncan S. Sutherland, and Fredrik Hk

J. Am. Chem. Soc., **2005**, 127 (14), 5043-5048• DOI: 10.1021/ja043672o • Publication Date (Web): 15 March 2005

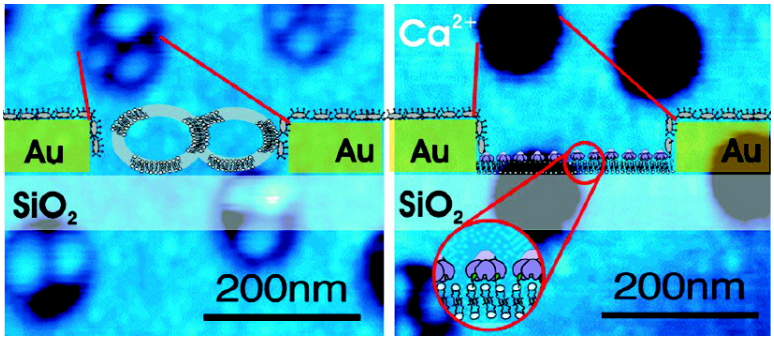

More About This Article

Additional resources and features associated with this article are available within the HTML version:

- Supporting Information
- Links to the 18 articles that cite this article, as of the time of this article download
- Access to high resolution figures
- Links to articles and content related to this article
- Copyright permission to reproduce figures and/or text from this article

View the Full Text HTML

J|A|C|S
ARTICLES
Published on Web 03/15/2005

Localized Surface Plasmon Resonance Sensing of Lipid-Membrane-Mediated Biorecognition Events

Andreas Dahlin,† Michael Zäch, Tomas Rindzevicius, Mikael Käll, Duncan S. Sutherland, and Fredrik Höök*

Contribution from the Department of Applied Physics, Chalmers University of Technology, SE-412 96 Göteborg, Sweden

Received January 18, 2005; E-mail: fredrik.hook@ftf.lth.se

Abstract: Supported phospholipid bilayers (SPBs) have emerged as important model systems for studies of the natural cell membrane and its components, which are essential for the integrity and function of cells in all living organisms, and also constitute common targets for therapeutic drugs and in disease diagnosis. However, the preferential occurrence of spontaneous SPB formation on silicon-based substrates, but not on bare noble-metal surfaces, has so far excluded the use of the localized surface plasmon resonance (LSPR) sensing principle for studies of lipid-membrane-mediated biorecognition reactions. This is because the LSPR phenomenon is associated with, and strongly confined to, the interfacial region of nanometric noble-metal particles. This problem has been overcome in this study by a self-assembly process utilizing localized rupture of phospholipid vesicles on silicon dioxide in the bottom of nanometric holes in a thin gold film. The hole-induced localization of the LSPR field to the voids of the holes is demonstrated to provide an extension of the LSPR sensing concept to studies of reactions confined exclusively to SPB-patches supported on SiO_2. In particular, we emphasize the possibility of performing label-free studies of lipid-membrane-mediated reaction kinetics, including the compatibility of the assay with array-based reading ($\sim 7 \times 7\ \mu m^2$) and detection of signals originating from bound protein in the zeptomole regime.

Introduction

As the focus in life sciences is shifting from genomics to proteomics, there is an intensive search for new sensor concepts compatible with real-time, label-free, and array-based protein analysis. As progress is made in these directions—which is not limited to new sensor concepts alone, but also includes sophisticated surface modification and the development of novel fluidic devices—high-throughput studies of low-abundant compounds in small volumes will ultimately become feasible. Considering the sensor elements in such devices, the sensitivity of the optical extinction band of subwavelength noble-metal particles to local changes in the interfacial refractive index (RI) deserves special attention.[1−5] Indeed, the sensitivity of the LSPR phenomenon to biomolecular recognition reactions has been proven compatible with *single* metal particle resolution, and the small size of the nanoparticles implies that binding of *zeptomoles* of protein is sufficient for signal detection.[6,7] This, combined with the facts that (i) the high sensitivity is reached without the introduction of external labels, which is generally complicated in the case of proteins, and (ii) recording of the temporal variation in the spectra provides information about binding kinetics, which is critical for reliable concentration determinations, means that the concept fulfills the requirements of the sensor elements foreseen in the affinity-based protein-analysis devices of the future.

However, hitherto no solutions have, to the best of our knowledge, demonstrated the use of the LSPR sensing concept for studies of cell-membrane-mediated reactions, which play essential roles in all living organisms. In the search for an in-depth understanding of cell-membrane-mediated reactions, including disease diagnosis and drug development, SPBs have been proven to be particularly valuable model systems,[8] well-suited for analysis using conventional surface plasmon resonance (SPR) analysis (see ref 9 and references therein). Still, significant efforts are currently being focused on new sensing concepts compatible with studies of cell-membrane-mediated reactions, as recently illustrated, for example, by methods based on colloidal phase transitions of lipid-membrane-coated silica beads,[10] biorecognition-induced reorganization of phospholipid-coated

* Current address of corresponding author: Division of Solid State Physics, Lund University, SE-221 00 Lund, Sweden.
† Current address: Division of Solid State Physics, Lund University, SE-221 00 Lund, Sweden.

(1) Hutter, E.; Fendler, J. H. *Adv. Mater.* **2004**, *16* (19), 1685−1706.
(2) Penn, S. G.; He, L.; Natan, M. J. *Curr. Opin. Chem. Biol.* **2003**, *7* (5), 609−615.
(3) Elghanian, R.; Storhoff, J. J.; Mucic, R. C.; Letsinger, R. L.; Mirkin, C. A. *Science* **1997**, *277* (5329), 1078−1081.
(4) Haes, A. J.; Stuart, D. A.; Nie, S. M.; Van Duyne, R. P. *J. Fluoresc.* **2004**, *14* (4), 355−367.
(5) Lahav, M.; Vaskevich, A.; Rubinstein, I. *Langmuir* **2004**, *20* (18), 7365−7367.
(6) McFarland, A. D.; Van Duyne, R. P. *Nano Lett.* **2003**, *3* (8), 1057−1062.
(7) Raschke, G.; Kowarik, S.; Franzl, T.; Sonnichsen, C.; Klar, T. A.; Feldmann, J.; Nichtl, A.; Kurzinger, K. *Nano Lett.* **2003**, *3* (7), 935−938.
(8) Sackmann, E. *Science* **1996**, *271* (5245), 43−48.
(9) Cooper, M. A. *J. Mol. Recognit.* **2004**, *17* (4), 286−315.
(10) Baksh, M. M.; Jaros, M.; Groves, J. T. *Nature* **2004**, *427* (6970), 139−141.

liquid crystals,[11] and membrane-protein-containing lipid membranes on planar Au. [12] However, the fact that even planar noble-metal surfaces (e.g. Au or Ag) require extensive chemical modification for SPBs to be created[13−15] means that the LSPR concept is not directly compatible with studies of this kind. In addition, the evanescent field associated with the surface plasmons vanishes exponentially from the interfacial region, with a typical decay length of 10−20 nm.[16] This, in turn, limits the applicability of the concept to tethered lipid vesicles[17,18] or, for that matter, SPBs supported on top of immobilized polymer cushions.[19]

We have circumvented the previous constraint of the LSPR sensing concept to gold-based surface modifications, which has generally utilized thiolated compounds,[1−5] by introducing a substrate that is, in principle, the inverse of supported noble-metal particles, namely cylindrical (∅ ∼ 110 nm) holes in a thin (20 nm) Au film supported on a planar SiO_2 substrate. Although the role played by *surface plasmons* in the "resonant surface plasmon enhanced transmission" phenomenon observed for ordered arrays of nanometeric holes in optically thick (opaque) noble-metal films[16,20] was recently challenged,[21] similar hole-based templates have previously been used for biomolecular sensing reactions,[22] although still restricted to reactions at the liquid−metal interface. Since the hole-structure utilized in the present study was created through colloidal lithography, long-range high-order diffractive coupling effects are efficiently avoided.[23] Instead, as a consequence of the optically thin (transparent) gold film, the LSPR associated with the polarization of a cylindrical void, with a field strongly localized in the holes,[24] appears as a resonance peak in *extinction* mode. The high degree of confinement of the LSPR field to the voids of the holes is demonstrated to facilitate the analysis of lipid-membrane-mediated biorecognition reactions restricted to SPB patches localized at the SiO_2 bottom of the holes, rather than the surrounding metal (Au) region.

The surface modification protocol was established using quartz crystal microbalance with dissipation (QCM-D) monitoring, and the localized SPB formation at the SiO_2 bottom of the holes was verified using atomic force microscopy (AFM). Measurements of biomolecular recognition on the SPB patches were performed using vis-NIR optical extinction spectroscopy in transmission mode, and the compatibility of the concept with array-based reading with a lateral resolution better than 10×10 μm^2 (<600 holes) was verified using dark field microscopy (DFM).

Experimental Section

General information. Water was deionized and filtered (MilliQ unit, Millipore). The ssDNA molecules used were 5′-TAT-TTC-TGA-TGT-CCA-AGC−CAC-GAG-TTC-3′ (DNA_A), 5′-GAA-CTC-GTG-GCT-3′ (DNA_B), 5′-TGG-ACA-TCA-GAA-ATA-3′ (DNA_C), and 5′-TGT-ACG-TCA-CAA-CTA-3′ (DNA_D), with DNA_A and DNA_B derivatized with cholesterol (separated with a CCC spacer) at the 3′- and 5′-ends, respectively, and with DNA_C and DNA_D derivatized with biotin (CCC separated) at the 3′-end (MedProbe). Stock solutions of DNA strands (20 μM in 10 mM Tris, 1 mM EDTA, pH 8.0); the proteins biotin-labeled BSA (Sigma, 1 mg/mL in water), NeutrAvidin (Pierce, 1 mg/mL in water), and cholera toxin AB_5 (Sigma-Aldrich, 1 mg/mL in water); and the lipids 1-palmitoyl-2-oleoyl-*sn*-glycero-3-phosphocholine (POPC, 25 mg/mL in $CHCl_3$), biotinylated 1,2-dipalmitoyl-*sn*-glycero-3-phosphoethanolamine (biotin−PE, 25 mg/mL in $CHCl_3$), both from Avanti Polar Lipids, and ganglioside G_{M1} lipids (Sigma-Aldrich, 25 mg/mL in 30 vol % methanol in $CHCl_3$) were stored at −20 °C, except for cholera toxin, which was stored at 4 °C. Lipid vesicles were prepared by evaporation of the solvent under N_2 (>1 h), followed by hydration in buffer (10 mM Tris, 100 mM NaCl, pH 8.0, to a final concentration of 5 mg/mL), and extrusion through 0.1 and 0.03 μm polycarbonate membranes (21 times per filter size, Whatman, UK) and were stored at 4 °C under N_2. For biotin−lipid- and G_{M1}-modified vesicles, 5 wt % of the modified lipid was introduced before evaporating the solvent. All experiments were performed by dissolving the stock solutions in buffer to the given concentrations. For a Ca^{2+}- or EDTA-containing buffer, 10 mM $CaCl_2$ or EDTA was included for the normal buffer. The substrates for preparation of the nanostructured samples were 300 μm quartz disks (MaxTek Inc.) and the Au- and SiO_2-coated QCM crystals were polished 5 MHz crystals (Q-Sense AB, Sweden). The nanostructured substrates and QCM crystals were cleaned between each experiment with a 1 wt % SDS solution for ∼16 h, UV−ozone treatment for ∼1 h, and rinsing in water (Milli-Q grade, Millipore, US) for ∼3 h before drying with N_2. Although good reproducibility (within 10%) was achieved between different samples, the data presented all come from repeated experiments (reproducibility within 5%) performed on the same sample.

Substrate Preparation. Colloidal lithography was used to fabricate 110-nm-diameter holes in a 20-nm-thick gold film on 1-in.-diameter single quartz substrates as described elsewhere.[25] Briefly, electrostatic self-assembly was used to produce a colloidal monolayer mask (110 ± 4.5 nm diameter sulfate-modified polystyrene latex, IDC) which was used here in a lift-off procedure to deposit a 20-nm-thick gold film, preceded by thermal evaporation of a 0.5 nm Ti adhesive layer (both electron beam heated, at a rate of 0.1 nm/s at a pressure of 1.5×10^{-6} Torr, AVAC HVC-600). The colloidal particles were removed by tape stripping, leaving ∼13 holes/μm^2 in a contiguous gold film over the whole quartz substrate.

AFM. All AFM measurements were carried out in liquid with a PicoPlus large-area scanner fitted onto a PicoSPM microscope (Molecular Imaging Inc.). Cantilevers (MicroLevers type MSCT-NONM, Veeco Europe) were cleaned in 1 wt % SDS solution and subsequently water and calibrated using the thermal noise method.[26] Cantilevers with spring constants (k) of ∼0.01 or ∼0.03 N/m were used. The imaging force was carefully adjusted to its minimum value, which, depending on the spring constant of the applied cantilever, is on the order of 100−300 pN. A scanning probe image processor (Image Metrology Inc., Denmark) was used to plane-fit the images, to calculate the image histograms, and to convert deflection vs z-position data into force vs distance curves.

(11) Brake, J. M.; Daschner, M. K.; Luk, Y. Y.; Abbott, N. L. *Science* **2003**, *302* (5653), 2094−2097.
(12) Ataka, K.; Giess, F.; Knoll, W.; Naumann, R.; Haber-Pohlmeier, S.; Richter, B.; Heberle, J. *J. Am. Chem. Soc.* **2004**, *126*, 16199−16206.
(13) Heyse, S.; Ernst, O. P.; Dienes, Z.; Hofmann, K. P.; Vogel, H. *Biochemistry* **1998**, *37* (2), 507−522.
(14) Giess, F.; Friedrich, M. G.; Heberle, J.; Naumann, R. L.; Knoll, W. *Biophys. J.* **2004**, *87* (5), 3213−3220.
(15) Ekeroth, J.; Konradsson, P.; Hook, F. *Langmuir* **2002**, *18* (21), 7923−7929.
(16) Barnes, W. L.; Dereux, A.; Ebbesen, T. W. *Nature* **2003**, *424* (6950), 824−830.
(17) Yoshina-Ishii, C.; Boxer, S. G. *J. Am. Chem. Soc.* **2003**, *125* (13), 3696−3697.
(18) Pfeiffer, I.; Hook, F. *J. Am. Chem. Soc.* **2004**, *126* (33), 10224−10225.
(19) Wagner, M. L.; Tamm, L. K. *Biophys. J.* **2000**, *79* (3), 1400−1414.
(20) Ebbesen, T. W.; Lezec, H. J.; Ghaemi, H. F.; Thio, T.; Wolff, P. A. *Nature* **1998**, *391* (6668), 667−669.
(21) Lezec, H. J.; Thio, T. *Opt. Express* **2004**, *12* (16), 3629−3651.
(22) Brolo, A. G.; Gordon, R.; Leathem, B.; Kavanagh, K. L. *Langmuir* **2004**, *20* (12), 4813−4815.
(23) Hanarp, P.; Kall, M.; Sutherland, D. S. *J. Phys. Chem. B* **2003**, *107* (24), 5768−5772.
(24) Prikulis, J.; Hanarp, P.; Olofsson, L.; Sutherland, D.; Kall, M. *Nano Lett.* **2004**, *4* (6), 1003−1007.
(25) Hanarp, P.; Sutherland, D. S.; Gold, J.; Kasemo, B. *Colloids Surf. A-Physicochem. Eng. Aspects* **2003**, *214* (1−3), 23−36.
(26) Hutter, J. L.; Bechhoefer, J. *Rev. Sci. Instrum.* **1993**, *64* (7), 1868−1873.

QCM-D. A quartz crystal microbalance with dissipation monitoring (Q-Sense AB, Sweden), described in detail elsewhere,[27,28] was used to verify the surface modification steps on planar macroscopic SiO_2 and Au surfaces.

Extinction Spectroscopy. The nanostructured sample was mounted in a liquid exchange cell with a total volume of ~110 μL, placed adjacent to the cuvette holder in a spectrophotometer (Cary500, Varian), perpendicular to the incoming light beam. The area probed was ~60 mm^2, corresponding to ~7.6×10^8 holes. Extinction spectroscopy measurements were carried out by rapidly (<1 s) exchanging the liquid within the cell, after which adsorption reactions were monitored from stagnant solution.

DFM. Elastic light scattering was recorded using dark-field microscopy with a liquid-exchange cell similar to the one used for extinction mode experiments. In brief, white light from a 100 W halogen lamp was guided through a DF condenser (Nikon dry, numerical aperture (NA) = 0.95−0.80) on an inverted microscope (Nikon TE300), and the sample was illuminated at an angle larger than the collection angle of the objective (Nikon 60×/NA = 0.7). The scattered light was collected using a 400 μm optical fiber and recorded using a grating spectrometer (AvaSpec-2048, Avantes), with a collection area of 49 μm^2.

Results and Discussion

AFM Evaluation of the Sensor Template. The sensor template, composed of nanometric SPB patches confined to the SiO_2 bottom of the holes, was obtained by first utilizing the preference of biotin-modified bovine serum albumin (biotin−BSA) to adsorb on Au rather than SiO_2.[29] In this way, the Au region becomes inert to lipid vesicle adsorption, while the weak adsorption of biotin−BSA to SiO_2 leaves the substrate within the holes potentially available for SPB formation.[30] However, contact-mode AFM scans following the subsequent biotin−BSA and lipid vesicle adsorption clearly showed the formation of assemblies resembling intact vesicles, rather than planar SPBs, in the majority (>95%) of the holes (Figure 1A). This shows that the spatial constraints imposed by the comparable dimensions of holes (Ø ~ 110 nm) and vesicles (Ø ~ 40 nm) hamper spontaneous bilayer formation. In strong contrast, by instead performing the vesicle adsorption step in a buffer containing Ca^{2+} (10 mM $CaCl_2$), which is known to promote spontaneous SPB formation on macroscopic substrates,[31] preferential formation of smooth planar bilayer patches was observed in the vast majority of holes (>95%) (Figure 1B). This observation was confirmed by an evaluation of height histograms from scans of the nanohole structure before and after subsequent exposures to biotin−BSA and vesicles in the presence of Ca^{2+} (Figure 1C). The observed changes in height difference between the Au film and the SiO_2 holes, obtained by fitting Gaussian functions to the histogram peaks, were ~+1.7 nm upon exposure of the surface to biotin−BSA and ~−5.0 nm upon the addition of vesicles. These values are considered consistent with monolayer adsorption of biotin−BSA on Au and SPB formation in the SiO_2 holes, respectively. Further evidence of SPB formation at the bottom of the holes was provided by force-versus-distance curves acquired upon tip-approach AFM both

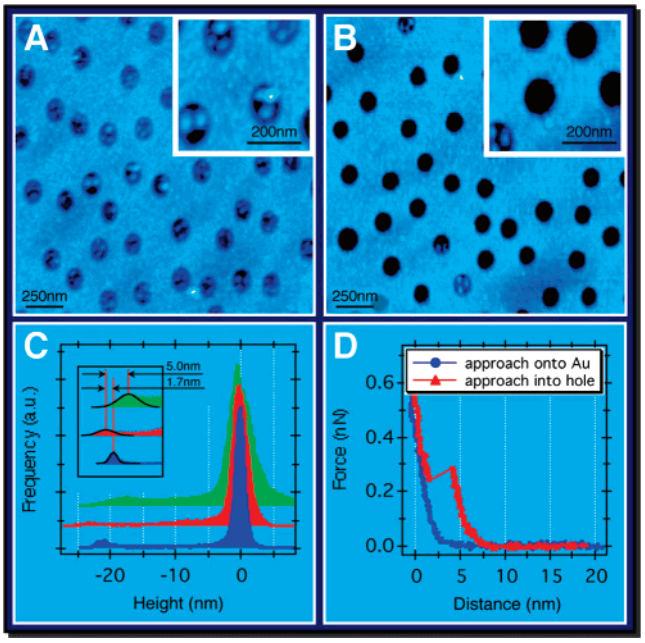

Figure 1. AFM topography scans of the nanohole structure after exposure to biotin−BSA (~0.3 μM) and vesicles (Ø ~ 40 nm, lipid concentration ~100 μg/mL), in buffer, in the absence (A) and presence (B) of Ca^{2+} (10 mM $CaCl_2$). The *z*-ranges are 37 and 38 nm (35 and 25 nm) for the main images (insets) in A and B, respectively. Panel C shows the height histograms of scans of the original nanohole structure (blue), the nanohole structure after exposure to biotin−BSA (red), and vesicles in the presence of Ca^{2+} (green). The inset shows an enlargement of the weaker peaks on the left-hand side of the main figure, including Gaussian fits to these peaks. Panel D shows representative force vs distance curves as acquired upon approach on the gold regions (blue) and into the holes (red) of the nanohole structure after treatment with biotin−BSA and vesicles in the presence of Ca^{2+}.

in the holes and on the Au film, which were characterized by the presence or absence of a distinct discontinuity, respectively (Figure 1D). The discontinuity observed for the holes, typically at an applied force between 0.1 and 0.4 nN, is indicative of a lipid bilayer.[32] Note that we only observed one discontinuity, in contrast to two discontinuities recently reported.[32] The difference between the two cases, according to our interpretation, is that, due to a limited supply of lipid material in our case, no bilayer was formed on the tip. This interpretation is supported by the fact that we did not observe a discontinuity on the gold (using forces up to 5 nN).

A significant effect of the presence of Ca^{2+} on the vesicle adsorption kinetics was also observed in QCM-D measurements on planar macroscopic SiO_2 substrates (Figure 2). Significantly, the amplitudes of the peaks in resonance frequency (*f*, cf. adsorbed mass) and dissipation (*D*, cf. rigidity), which comprise a signature of the vesicle coverage at which the bilayer formation is initiated,[30] are much lower in the presence of Ca^{2+} and appear earlier. This is in analogy to the promotion of SPB formation previously observed at increased temperature and osmotic pressure,[33] thus confirming the influence from Ca^{2+} as observed in AFM (Figure 1). This conclusion is also verified by the ability to successfully image adsorbed vesicles both in the absence and the presence of Ca^{2+} (Figure 1A,B), which indicates that the observed SPB patches were not tip-induced. The significant

(27) Rodahl, M.; Hook, F.; Krozer, A.; Brzezinski, P.; Kasemo, B. *Rev. Sci. Instrum.* **1995**, *66* (7), 3924−3930.
(28) Hook, F.; Rodahl, M.; Kasemo, B.; Brzezinski, P. *Proc. Natl. Acad. Sci. U.S.A.* **1998**, *95* (21), 12271−12276.
(29) Svedhem, S.; Pfeiffer, I.; Larsson, C.; Wingren, C.; Borrebaeck, C.; Hook, F. *Chembiochem* **2003**, *4* (4), 339−343.
(30) Keller, C. A.; Kasemo, B. *Biophys. J.* **1998**, *75* (3), 1397−1402.
(31) Reviakine, I.; Brisson, A. *Langmuir* **2000**, *16* (4), 1806−1815.
(32) Richter, R.; Mukhopadhyay, A.; Brisson, A. *Biophys. J.* **2003**, *85* (5), 3035−3047.
(33) Reimhult, E.; Hook, F.; Kasemo, B. *Langmuir* **2003**, *19* (5), 1681−1691.

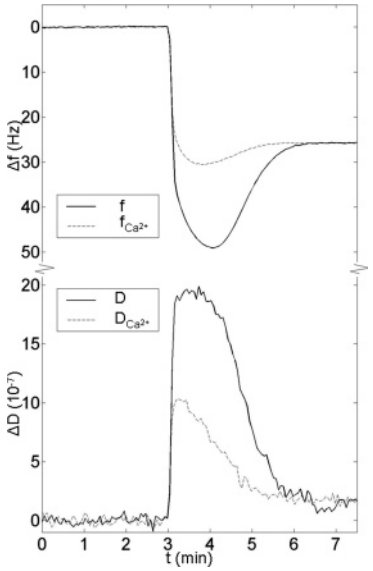

Figure 2. Changes in resonance frequency, *f*, and energy dissipation, *D*, versus time obtained from QCM-D measurements upon exposure of a SiO_2 substrate to lipid vesicle suspensions (~100 μg/mL, $\varnothing \sim 40$ nm in buffer) in the absence and presence of Ca^{2+} (10 mM $CaCl_2$).

differences observed in optical extinction data also support this conclusion (see below).

Optical Characterization of the Surface Modification. Inspired by these results, optical extinction spectroscopy, $\epsilon(\lambda)$, was used to characterize changes in the optical properties of the nanostructured substrate induced upon changes in both bulk (suspension-induced) and local (binding-induced) refractive index.

Figure 3A shows the extinction spectrum (300 nm $< \lambda <$ 1000 nm) of the pure substrate in buffer with the LSPR peak, λ_{peak}, at ~685 nm, in agreement with previous observations.[24] Extinction spectra were recorded for linear changes in bulk RI using glycerol/water suspensions (Figure 3B), resulting in a linear increase in both λ_{peak} and the peak extinction value, ϵ_{peak} (Figure 3C). These results are in good agreement with previous results for nanoparticle LSPRs[6,23,34]. Traditionally, the sensitivity of the LSPR peak to changes in bulk refractive index is expressed as $\Delta\lambda_{peak}$ per unit bulk RI, which in the present case yields a sensitivity of 180 $\pm$ 10 nm/RI. However, the highest absolute sensitivity to changes in RI (signal-to-noise ratio) was obtained by recording the changes in extinction at the longer wavelength inflection point ($\lambda \sim 725$ nm) of the extinction peak (Figure 3A), at which the absolute change in ϵ was observed to have its maximum. The extinction-based sensitivity at this wavelength was approximately one absorbance unit per unit RI, with a resolution in ϵ better than 10^{-4} at $\lambda \sim 725$ nm for sampling rates >1s.

The spectral changes induced upon addition of biotin−BSA, which binds to Au only, followed by the addition of lipid vesicles in the absence or presence of Ca^{2+} (see Figure 1) are shown in Figure 3D. Detailed inspection of this plot reveals several interesting features. First, note that the $\Delta\epsilon_{max}/\Delta\lambda_{peak}$ ratio (solid lines) differs for the different binding reactions and that it is in all cases larger than that obtained for changes in bulk RI (dashed arrow and Figure 3B,C). Although a conclusive

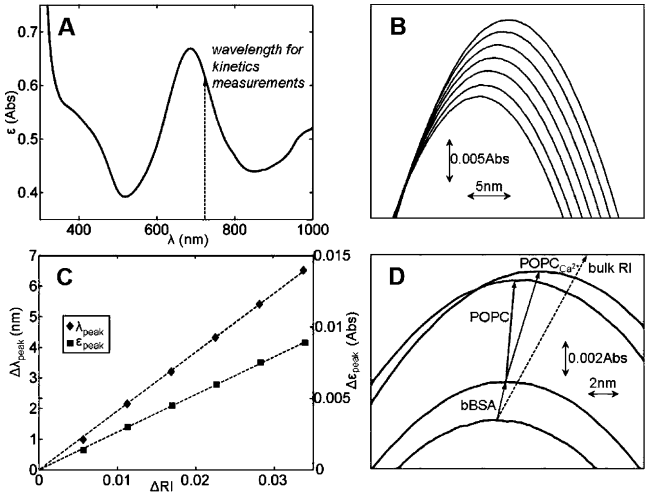

Figure 3. (A) Extinction (ϵ) spectrum of the pure substrate in buffer. The arrow indicates the longer wavelength inflection point used for kinetics data. (B) Changes in the extinction peak height/position upon increasing glycerol concentration ($V_{glycerol} = 5, 10, ..., 35\%$). (C) Changes in extinction peak height (ϵ_{peak}) and peak position (λ_{peak}) versus change in bulk refractive index (ΔRI) achieved using the glycerol suspensions. λ_{peak} and ϵ_{peak} were determined by a parabolic fit to the linear gradient region of the spectrum and the RI dependence of volume percent glycerol in water was determined with conventional surface plasmon resonance.[41] The dashed lines are linear least-squares fits to the data. [Changes in extinction at the longer wavelength inflection point, $\lambda \sim 725$ nm, which were used to record binding kinetics (see below), also scaled linearly with bulk RI (data not shown)]. (D) Asymptotic changes in the LSPR extinction peak with respect to a bare sample in buffer (lower curve) upon addition of first biotin−BSA (~0.3 μM, bBSA) followed by rinsing and addition of POPC phospholipid vesicles (~100 μg/mL, $\varnothing \sim 40$ nm) in the absence (POPC) and presence ($POPC_{Ca^{2+}}$) of Ca^{2+} (10 mM $CaCl_2$). EDTA (10 mM) was used to remove Ca^{2+} prior to recording the latter spectrum. Also indicated are the relative changes in extinction and peak position for the biomolecular binding (solid lines) and for changes in bulk refractive index (dashed line) (cf. C).

statement requires a complete theoretical description of the LSPR field associated with a randomized hole structure of the kind utilized in this study, it appears likely that the observation originates from a nonhomogeneous macromolecular distribution within the LSPR field. Note, in particular, the significant difference observed upon the addition of lipid vesicles in the two cases, demonstrating the formation of lipid assemblies adopting different structures depending on whether Ca^{2+} is present or not. Second, despite the fact that the AFM images suggest a higher lipid content per hole for nonruptured vesicles (in the absence of Ca^{2+}) than for the planar SPB patches (in the presence of Ca^{2+}), the magnitude of the changes in extinction are higher in the latter case. The most likely explanation of these two observations is that bilayer patches confine lipid mass to regions of higher LSPR field strength, i.e., at the bottom of the hole. Third, although Au constitutes ~89% (the walls included) and SiO_2 only ~11% of the available surface area, the magnitude of the changes observed upon the addition of lipid vesicles is up to a factor of ~3 higher than that observed for biotin−BSA. Assuming a similar refractive index and mass deposition per unit surface area, this suggests that the holes, rather than the gold, should be utilized for optimal sensitivity in sensor applications with this template.

Evaluation of the Sensor Template for Studies of Membrane-Mediated Biorecognition Reactions. Encouraged by the high confinement of the LSPR field to the holes, and the high symmetry of SPB patches formed in the presence of Ca^{2+}, a series of experiments was performed to evaluate the sensor

(34) Mitsui, K.; Handa, Y.; Kajikawa, K. *Appl. Phys. Lett.* **2004**, *85* (18), 4231−4233.

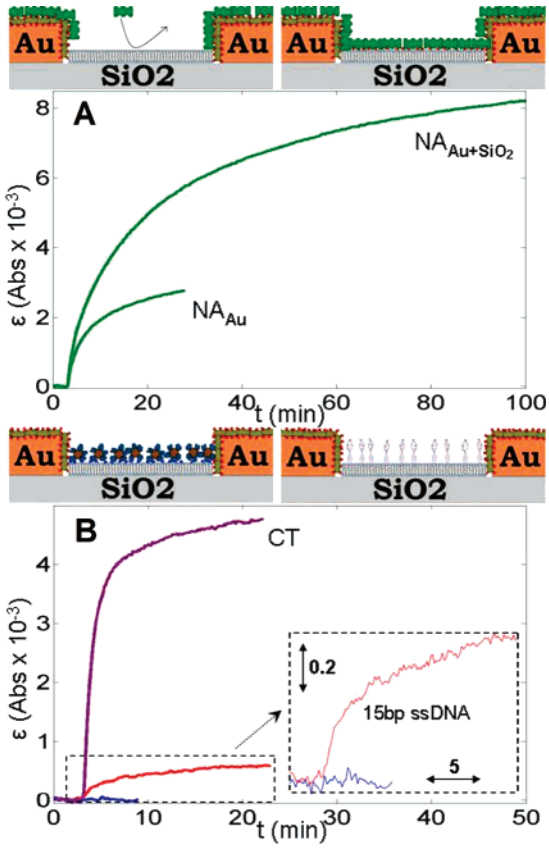

Figure 4. (A) Temporal variation in extinction measured at the longer wavelength inflection point (~725 nm) of the LSPR peak (cf. Figure 2A) upon addition of NeutrAvidin, (NA, ~0.3 μM). In both cases, Au is modified with biotin−BSA. In one case, biotin-modified SPB patches cover the SiO_2 regions (NA_{Au+SiO_2}), while in the other, bare SPB patches cover the SiO_2 regions (NA_{Au}). (After SPB formation, EDTA (10 mM) was added to remove Ca^{2+} prior to subsequent additions) (B) Addition of cholera toxin (CT, ~0.5 μM) to G_{M1}-modified (5w%) SPBs. The inset shows a magnification of changes in extinction versus time upon addition of a 15-base long noncomplementary (0.2 μM, blue) and a fully complementary strand (0.2 μM, red) to SPB patches modified with a DNA construct carrying two cholesterol moieties at its one end and a 15-base-long single strand available for hybridization at the other.[18]

template in terms of binding reactions confined to the SPB patches. However, initially the template composed of biotin−BSA on Au and SPB patches on SiO_2 was used to evaluate not only the overall sensitivity of the sensor but also the relative strength of the field distribution on Au and at the bottom of the holes. Upon addition of the biotin-binding protein NeutrAvidin (a streptavidin analogue), the sensitivity of the Au regions could be compared to that of the SPB patches by including a fraction (5%) of biotin-modified lipids in the vesicles used for bilayer formation.[35] Since a SPB composed of POPC lipids only is inert toward protein adsorption, and since the coverage (per unit surface area) of NeutrAvidin is similar on biotin−BSA and biotin-modified SPBs (supported by QCM-D, data not shown), the addition of NeutraAvidin to these two templates would in one case yield binding to biotin−BSA on Au only and in the other binding to the whole template. Figure 4A shows the temporal variation in extinction at the ~725 nm inflection point for NeutraAvidin addition to a nanohole substrate modified with biotin−BSA and either pure SPBs or biotin-modified SPBs. Strikingly, the saturated change is more than a factor of 3 higher in the case of NeutrAvidin binding not only to the biotin−BSA coated Au regions but also to the biotin-modified SPBs on SiO_2. Assuming that the optical responses from binding to the different regions are independent, the fact that the effective SPB-coated area is less than 11% implies that the sensitivity of the latter regions is, in terms of mass-uptake per unit area, more than a factor of 16 higher than the Au region.

Inspired by this extremely high confinement of the sensitivity to the SPB patches, membrane-specific reactions were studied by first evaluating the binding of cholera toxin to ganglioside G_{M1} glycolipids (G_{M1}).[36] Figure 4B shows the same type of data as in part A upon addition of cholera toxin, illustrating the compatibility of the concept with naturally occurring membrane-mediated reactions. Note also that the magnitude of the asymptotic response to cholera toxin is in good agreement with the difference between NeutrAvidin binding to both Au and SiO_2 and Au only (see Figure 4A). QCM-D monitoring showed insignificant binding of cholera toxin to biotin−BSA-modified Au, pure SPBs, and SiO_2, verifying that the binding of cholera toxin was specific (data not shown).

To investigate the detection limit of the system, a cholesterol-modified DNA construct was incorporated into the SPB patches,[18] followed by the addition of noncomplementary and fully complementary 15-base (5 kDa) single-stranded DNA (inset in Figure 4B). Note that there is no binding of non-complementary DNA and that the rate of hybridization, known to be reaction-limited under these conditions,[35] is in good agreement with a single-exponential model. This suggests that although the contribution from individual molecules to the overall signal may vary depending on the location within the hole (see above), a sufficient number of molecules and/or holes provides a signal that is proportional to the number of bound molecules.

Compatibility of the Sensing Concept with Array-Based Reading. This means of controlling and recording the binding kinetics of membrane-mediated molecular recognition reactions on planar nanoscale lipid assemblies provides a new way to probe cell-membrane-associated reactions. The particular added value comes, however, from the straightforward way by which the detection concept can be transferred from the macroscopic to the microscopic domain, thus facilitating array-based reading. This possibility was illustrated by recording the spectrum of elastically scattered light from a 7×7 μm^2 (~600 holes) area using DFM.[7] Remarkably, a treatment identical to that shown in Figures 3D (for biotin-modified SPB patches enabling NeutrAvidin binding to the whole surface), followed by the addition of NeutrAvidin (or cholera toxin, not shown), resulted in asymptotic changes in height and position of the scattering peak (Figure 5) with relative values essentially identical to those observed in extinction mode. Assuming that the signal also in the scattering spectrum originates predominantly from the SPB patches, the number of bound proteins that give rise to the detected signal corresponds to less than 300 zmol.

In conclusion, this means that the concept comprises a sensor component which, when combined with appropriate fluidics, is likely to compete with the sensitivity of, for example, fluorescent-based array-reading techniques. There is, however, still room

(35) Larsson, C.; Rodahl, M.; Hook, F. *Anal. Chem.* **2003**, *75* (19), 5080−5087.

(36) Janshoff, A.; Steinem, C.; Sieber, M.; elBaya, A.; Schmidt, M. A.; Galla, H. J. *Eur. Biophys. J. Biophys. Lett.* **1997**, *26* (3), 261−270.

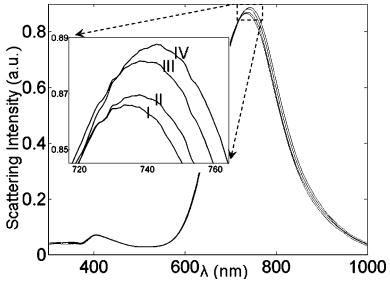

Figure 5. Changes in the LSPR peak from dark-field recordings of scattered light from a 7×7 μm^2 region (~600 holes) of the sample in (I) buffer, and the asymptotic spectra obtained upon subsequent binding of (II) biotin−BSA (~0.3 μM), (III) biotin-modified vesicles in the presence of Ca^{2+} (~100 μg/mL), and (IV) NeutrAvidin (~0.3 μM). The difference in LSPR peak position between extinction mode (~685 nm) and scattering mode (~730 nm) is expected.[24]

for further optimization by rational design of the surface structure to perfectly match the particular biomolecular recognition schemes employed, which will enhance both spatial and temporal resolution, as well as the overall sensitivity. Furthermore, new methods of this kind providing detailed information about binding reactions confined to nanoscale patches of supported membranes are likely to promote the understanding of several cell-membrane-related phenomena, such as lipid-phase separation and raft formation,[37] including the relation of such processes to the early stages of nucleation and growth of 2D protein domains/crystals.[38,39] Furthermore, the possibility to control the density of receptors in confined lipid areas is likely to facilitate studies of multivalent interactions, known to be responsible for most high-affinity interactions at cell membranes.[40]

Acknowledgment. The work was supported by the Biomimetic Material Science Program, funded by SSF, Sweden, the BioNanoIT Program, funded by Vinnova, Sweden and the Chalmers Bioscience Program.

JA043672O

(37) Binder, W. H.; Barragan, V.; Menger, F. M. *Angew. Chem. Int. Ed.* **2003**, *42* (47), 5802−5827.
(38) Venien-Bryan, C.; Lenne, P. F.; Zakri, C.; Renault, A.; Brisson, A.; Legrand, J. F.; Berge, B. *Biophys. J.* **1998**, *74* (5), 2649−2657.
(39) Wilson-Kubalek, E. M.; Brown, R. E.; Celia, H.; Milligan, R. A. *Proc. Natl. Acad. Sci. U.S.A.* **1998**, *95* (14), 8040−8045.
(40) Mammen, M.; Choi, S. K.; Whitesides, G. M. *Angew. Chem. Int. Ed.* **1998**, *37* (20), 2755−2794.
(41) Reimhult, E.; Larsson, C.; Kasemo, B.; Hook, F. *Anal. Chem.* **2004**, *76* (24), 7211−7220.